

Enzyme Catalysis *via* Control of Activation Entropy: Site-directed Mutagenesis of 6,7-Dimethyl-8-ribityllumazine Synthase

Markus Fischer^{1*}, Ilka Haase¹, Klaus Kis¹, Winfried Meining²
Rudolf Ladenstein², Mark Cushman³, Nicholas Schramek¹
Robert Huber⁴ and Adelbert Bacher¹

¹Institut für Organische Chemie und Biochemie Technische Universität München, Lichtenbergstr. 4 D-85747 Garching, Germany

²Karolinska Institute NOVUM Center for Structural Biochemistry, S-14157 Huddinge, Sweden

³Department of Medicinal Chemistry and Molecular Pharmacology, Purdue University, West Lafayette IN 47907, USA

⁴Abteilung Strukturforschung Max-Planck Institut für Biochemie, Am Klopferspitz 18a D-82512 Martinsried Germany

6,7-Dimethyl-8-ribityllumazine synthase (lumazine synthase) catalyses the penultimate step in the biosynthesis of riboflavin. In *Bacillus subtilis*, 60 lumazine synthase subunits form an icosahedral capsid enclosing a homotrimeric riboflavin synthase unit. The *ribH* gene specifying the lumazine synthase subunit can be expressed in high yield. All amino acid residues exposed at the surface of the active site cavity were modified by PCR assisted mutagenesis. Polar amino acid residues in direct contact with the enzyme substrates, 5-amino-6-ribitylamino-2,4(1*H*,3*H*)-pyrimidinedione and 3,4-dihydroxy-2-butanone 4-phosphate, could be replaced with relative impunity with regard to the catalytic properties. Only the replacement of Arg127, which forms a salt bridge with the phosphate group of 3,4-dihydroxy-2-butanone 4-phosphate, reduced the catalytic rate by more than one order of magnitude. Replacement of His88, which is believed to assist in proton transfer reactions, reduced the catalytic activity by about one order of magnitude. Surprisingly, the activation enthalpy ΔH^\ddagger of the lumazine synthase reaction exceeds that of the uncatalysed reaction. On the other hand, the free energy of activation ΔG^\ddagger of the uncatalysed reaction is characterised by a large entropic term ($T\Delta S^\ddagger$) of $-37.8 \text{ kJ mol}^{-1}$, whereas the entropy of activation ($T\Delta S^\ddagger$) of the enzyme-catalysed reaction is -6.7 kJ mol^{-1} . This suggests that the rate enhancement by the enzyme is predominantly achieved by establishing a favourable topological relation of the two substrates, whereas acid/base catalysis may play a secondary role.

© 2003 Elsevier Science Ltd. All rights reserved

*Corresponding author

Keywords: vitamin B₂; riboflavin biosynthesis; 6,7-dimethyl-8-ribityllumazine synthase; reaction mechanism; entropy of activation ΔS^\ddagger

Introduction

Vitamin B₂ (riboflavin) is biosynthesised by plants and numerous microorganisms, whereas animals depend on nutritional sources. Certain groups of eubacteria and yeast, including many important pathogens such as Enterobacteria, are unable to absorb riboflavin and its derivatives from the environment and are therefore absolutely dependent on endogenous synthesis of the vitamin.^{1,2} The enzymes of riboflavin biosynthesis may also be essential for Mycobacteria and for pathogenic yeasts.^{3–5} Thus, inhibitors of the ribo-

flavin pathway could serve as antibacterial and/or antimycotic drugs. The development of appropriate inhibitors could benefit from a detailed analysis of the structure and reaction mechanism of the riboflavin biosynthetic enzymes.

The biosynthetic pathway of riboflavin involves the formation of 5-amino-6-ribitylamino-2,4(1*H*,3*H*)-pyrimidinedione (**2**) from GTP *via* four reaction steps (Figure 1) (for review see Refs. 6–8). Riboflavin is then obtained from one equivalent of **2** and two equivalents of 3,4-dihydroxy-2-butanone 4-phosphate (**1**) in two sequential reaction steps catalysed by 6,7-dimethyl-8-ribityllumazine synthase (lumazine synthase) and riboflavin synthase. More specifically, 6,7-dimethyl-8-ribityllumazine synthase (lumazine synthase) catalyses a condensation reaction affording 6,7-dimethyl-8-ribityllumazine

Abbreviations used: PCR, polymerase chain reaction.
E-mail address of the corresponding author: markus.fischer@ch.tum.de

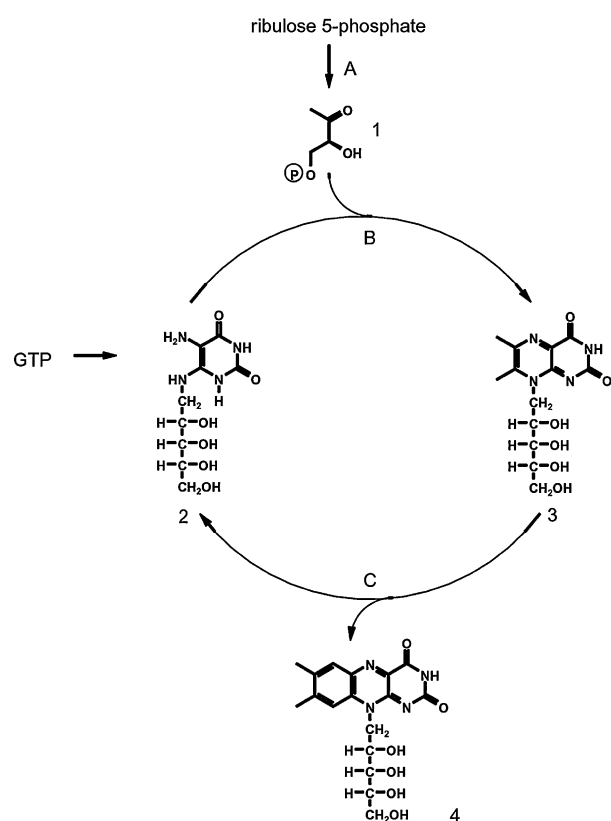


Figure 1. Terminal reactions in the pathway of riboflavin biosynthesis. (A) 3,4-dihydroxy-2-butanone 4-phosphate synthase; (B) lumazine synthase; (C) riboflavin synthase.

(3) and inorganic phosphate from 1 and 2.^{9,10} The lumazine 3 then undergoes an unusual dismutation affording riboflavin (4) and 2, which is catalysed by riboflavin synthase.^{11,12} The second product of that reaction, 5-amino-6-ribitylamino-2,4(1H,3H)-pyrimidinedione (2), is recycled as substrate of lumazine synthase.^{13,14}

In Bacillaceae, lumazine synthase and riboflavin synthase form a 1 MDa complex comprising an

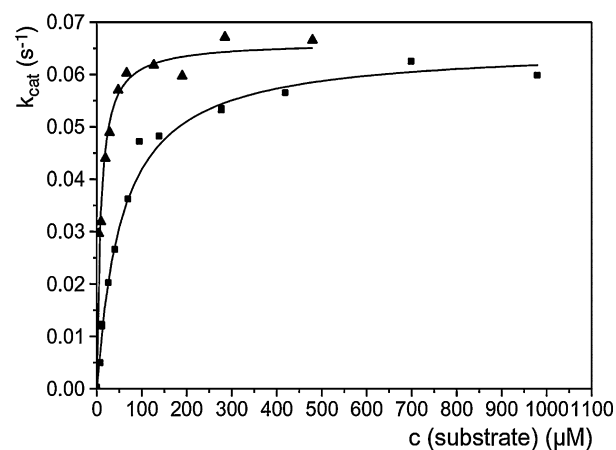


Figure 2. Saturation kinetic curve for 5-amino-6-ribitylamino-2,4(1H,3H)-pyrimidinedione (▲) and 3,4-dihydroxy-2-butanone 4-phosphate (■).

icosahedral capsid of 60 lumazine synthase subunits and a core of three riboflavin synthase subunits.^{15–17} The topological features of the bifunctional enzyme complex are conducive to enhanced overall reaction rates *via* substrate channeling under certain reaction conditions.¹⁸ Hollow icosahedral capsids consisting of 60 lumazine synthase subunits can be assembled *in vitro* after denaturation of the enzyme complex.¹⁹

The icosahedral lumazine synthase capsid of *Bacillus subtilis* has been studied in considerable detail by X-ray crystallography.^{17,20} It is best described as a dodecamer of pentamers. The 60 topologically equivalent active sites are all located at interface regions of adjacent subunits in the pentamer motif. Icosahedral lumazine synthases of *Aquifex aeolicus*²¹ and spinach²² and homopentameric lumazine synthases of *Saccharomyces cerevisiae*²³, *Schizosaccharomyces pombe*²⁴, *Brucella abortus*²⁵ and *Magnaporthe grisea*²² have also been studied by X-ray crystallography at high resolution.

In order to study the catalytic role of individual amino acid residues at the active site of *B. subtilis* lumazine synthase, all amino acid residues lining the catalytic cavity were subjected to saturation mutagenesis. Here, we report the impact of single amino acid replacements on the catalytic activity of the enzyme.

Results

A plasmid directing the expression of the *ribH* gene of *B. subtilis* under the control of a T5-promotor and *lac* operator was constructed as described in Materials and Methods. *E. coli* strains carrying this plasmid produced lumazine synthase subunits in high yield (approximately 10–20% of cell protein) as shown by SDS-polyacrylamide gel electrophoresis.

The recombinant protein was isolated as described in Materials and Methods. Steady state kinetic analysis showed a k_{cat} value of 0.056 s^{-1} in 100 mM potassium phosphate at pH 7.0, 5 mM EDTA and 37 °C. The K_M values for 3,4-dihydroxy-2-butanone 4-phosphate (1) and 5-amino-6-ribitylamino-2,4(1H,3H)-pyrimidinedione (2) were 55 μM and 9 μM , respectively (Figure 2, Table 3).

The recombinant protein sediments at an apparent velocity of 26 S. This is in agreement with data obtained for lumazine synthase capsids which had been reassociated *in vitro* in the presence of 5-nitro-6-ribitylamino-2,4(1H,3H)-pyrimidinedione (10a) from lumazine synthase subunits obtained by dissociation of the lumazine synthase/riboflavin synthase complex ($s = 26.3 \text{ S}$).¹⁵

Molecular mass determination of recombinant lumazine synthase by sedimentation equilibrium analysis yielded a value of 925 kDa (data not shown; calculated, 977 kDa). It follows that the recombinant subunits assemble *in vivo* under

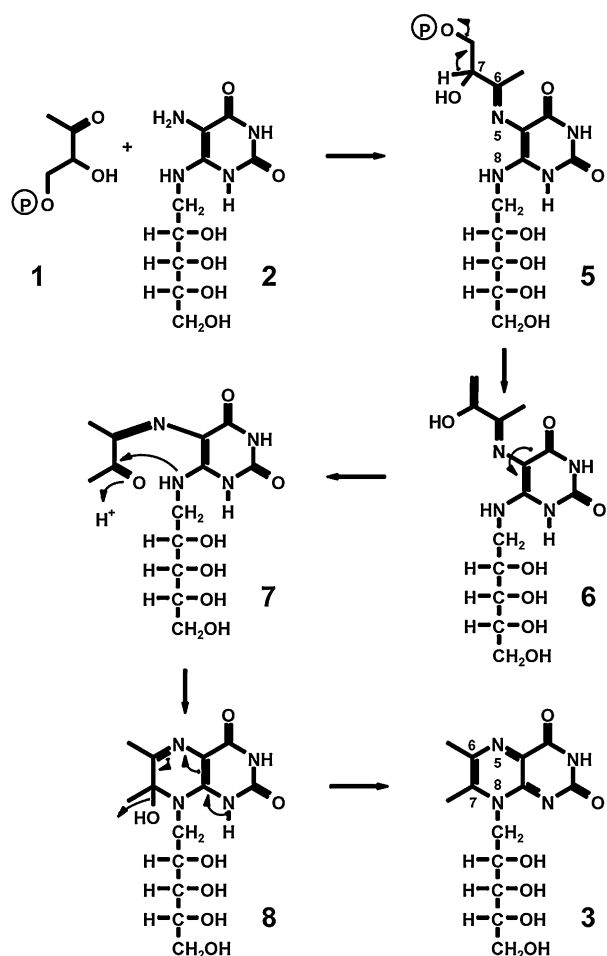


Figure 3. Hypothetical mechanism of lumazine synthase.

formation of icosahedral capsids, although the recombinant protein is devoid of the three riboflavin synthase subunits located in the core space of the wild-type enzyme.

The ultraviolet spectrum of recombinant lumazine synthase indicated that the preparation did not contain bound heterocyclic ligands in appreciable amounts. This suggests that the *in vivo* assembly of the icosahedral capsids proceeds with-

out the assistance of specific ligands, whereas the *in vitro* assembly of 60-meric capsids had been shown earlier to require the assistance of substrate analogues.¹⁹

A hypothetical reaction mechanism for lumazine synthase is summarised in Figure 3. Based on the experimentally determined regiospecificity of the reaction,¹⁰ it has been proposed that the first reaction step involves the formation of the Schiff base intermediate 5. The position 7 hydrogen atom of that hypothetical intermediate is activated by the imino motif, and deprotonation of the 7 carbon could facilitate the elimination of phosphate. Following the tautomerisation and rotation of the enol motif in the intermediate 6, the carbonyl group in 7 could be attacked by the position 8 amino group, yielding the hydrated pteridine structure 8. Dehydration of that unstable hydrate could afford 6,7-dimethyl-8-ribyllumazine (3).

This hypothetical mechanism suggests the involvement of several proton transfer reactions. Specifically, the formation of the Schiff base intermediate 5 could involve amino acid residues assisting the deprotonation of the nucleophilic nitrogen and/or protonation of the leaving OH group in the carbinolamine intermediate. Subsequent reaction steps could involve enzyme-assisted deprotonation at position 7 of the carbohydrate side-chain of 5 and/or deprotonation of the 8 nitrogen.

The involvement of His88 in the deprotonation of C-7 of intermediate 5 had been proposed on the basis of crystallographic data.¹⁷ Moreover, the keto/enol tautomerisation, the ring closure and the dehydration of the hypothetical intermediate 8 shown in Figure 3 are all candidates for enzyme-mediated proton transfer reactions. In order to analyse the role of specific amino acid residues in the hypothetical mechanism, we decided to mutagenise all amino acid residues that form part of the active site cavity surface.

The active site of lumazine synthase is known in considerable detail by crystallographic studies of the enzymes from *B. subtilis*, *S. cerevisiae*, *A. aeolicus*, spinach, *M. grisea*, *S. pombe* and *B. abortus* in complex with several substrate, intermediate or product analogues (Figure 4; the

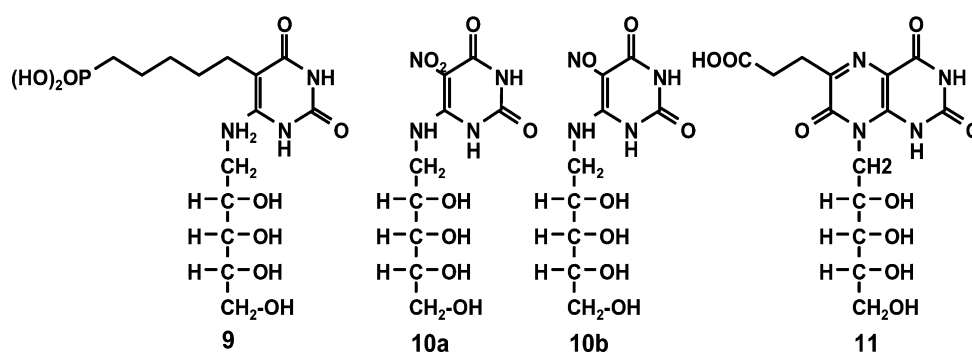


Figure 4. Enzyme inhibitors used in this study. 9, 5-(6-D-ribylamino-2,4-dihydroxypyrimidine-5-yl)-1-pentenyl-phosphonic acid; 10a, 5-nitro-6-ribylamino-2,4-(1H,3H)-pyrimidinedione; 10b, 5-nitroso-6-ribylamino-2,4-(1H,3H)-pyrimidinedione; 11, 6-carboxyethyl-7-oxo-8-ribyllumazine.

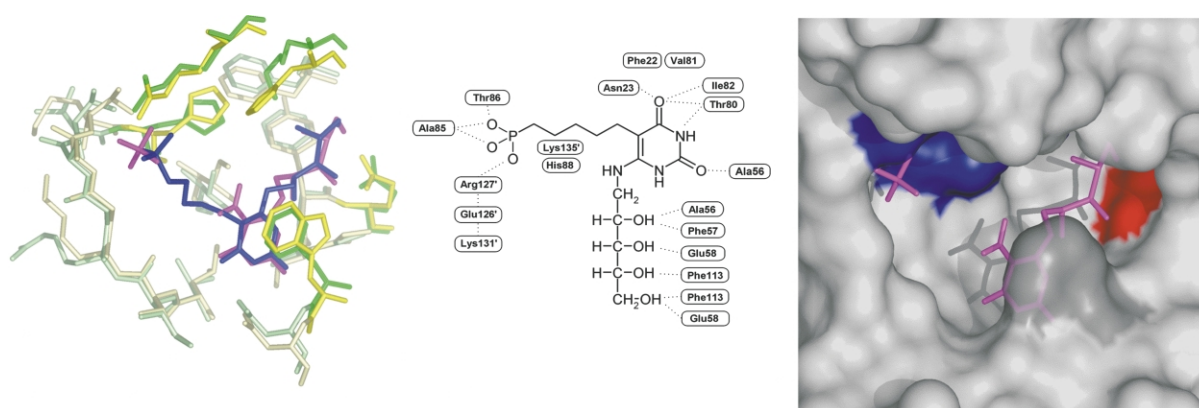


Figure 5. Active site topology of lumazine synthase. Left: comparison of the active sites of *B. subtilis* (LSBS) and *S. cerevisiae* (LSSC) lumazine synthase. For the alignment, only residues within a circumference of 10 Å around the pentylphosphonate inhibitor were used. Colour codes are as follows: labelled residues of LSSC: yellow; all other residues in LSSC: pale yellow; labelled residues of LSSC: green; all other residues in LSSC: pale green; 5-nitro-6-ribitylamino-2,4-(1*H*,3*H*)-pyrimidinedione and phosphate anion: blue; 5-(6-*D*-ribitylamino-2,4-dihydroxypyrimidine-5-yl)-1-pentylphosphonic acid: pink. Center: schematic representation of close contacts between the pentylphosphonate inhibitor and the LSBS active site after alignment. All contacts are derived from the alignment between LSBS and LSSC as described above. Ser142 und Asp138 lie in 4–8 Å distance to the ribityl side-chain at the entrance to the active site. Right: active site of *B. subtilis* lumazine synthase in complex with 5-nitro-6-ribitylamino-2,4-(1*H*,3*H*)-pyrimidinedione. Colour codes are as follows: Glu58, red; His88, Arg127, Lys131, blue; Phe22, grey. The Figure was generated with PYMOL Molecular Graphics System (W. D. Delano, 2002).

pyrimidine derivatives **10a** and **10b** are substrate analogues, the phosphonate derivative **9** is a close analogue of the proposed Schiff base intermediate **5**, and the 7-oxo lumazine derivative **11** is similar to the hypothetical hydrated lumazine intermediate **8**).^{20,22–25} The active site is a relatively large cavity located at the interface of adjacent subunits in the pentamer motif. Atoms pertaining to side-chains and/or main-chains of 22 amino acid residues form part of the surface of that cavity (Figure 5, Table 1).

Based on comparison of the conserved structural elements of all lumazine synthases and of enzyme-bound ligands whose structures have been determined crystallographically, the topology of reactants at the active site of the *B. subtilis* enzyme can be described as follows. The ribityl side-chain of the pyrimidine type substrate **10a** is bound in an extended conformation, which is closely similar in all available X-ray structures. The ribityl side-chain forms hydrogen bonds with the side-chain of Glu58 and with main-chain elements of Phe57 and Phe113 and is linked to Ser142 *via* a bridging water molecule. The pyrimidine ring forms a coplanar complex with an aromatic residue (phenylalanine in *B. subtilis*, *A. aeolicus* and spinach, and tryptophan in *S. cerevisiae*, *S. pombe*, *M. grisea* and *B. abortus*). In the enzyme from *B. subtilis*, the pyrimidine substrate is in coplanar van der Waals contact with the phenyl ring of Phe22. The coplanar complex was proposed to play an important mechanistic role by positioning the 5-amino groups of **2** for the electrophilic attack by the carbonyl group of **1**.²⁰ The pyrimidine ring forms hydrogen bonds with the Asn23 side-chain, the Ala56 peptide amide group and the Thr80 main-chain oxygen atom.

The phosphonate type inhibitor **9** is a close structural analogue of the hypothetical reaction intermediate **5**. In the complex with the enzyme from *S. cerevisiae*, the pentylphosphonate side-chain assumes an extended conformation, and the phosphonate group forms an ion pair with Arg136 to which it is also hydrogen bonded.²³ That conformation of the hypothetical intermediate **5** had been anticipated early on because the lumazine synthase of *B. subtilis* showed a fixed inorganic phosphate residue complexed to Arg127. His97 of the enzyme from *S. cerevisiae*, which is topologically equivalent to His88 in *B. subtilis* lumazine synthase, is close to the pentyl moiety of the intermediate analogue. Thus, it must appear as a candidate for proton transfer steps involved in the elimination of phosphate from **5** and/or the subsequent enolisation reaction.

All amino acid residues in direct contact with the substrates/intermediates *via* side-chain and/or backbone contacts were subjected to site-directed mutagenesis. A total of 58 single amino acid replacements were obtained by PCR mutagenesis as described in Materials and Methods. Briefly, two initial PCR amplifications were performed, one for the creation of the mutation and the other for the preparation of a template for the 3' extension of the mutagenised fragment. After removing the primers by gel electrophoresis, a second PCR step was carried out using the amplicates in an overlapping self-priming reaction yielding the entire 3' extended mutagenised *ribH* gene. Re-amplification using flanking outside primers afforded sufficient material for cloning.

One to nine different mutations were introduced at each site under study (Tables 2 and 7). Typically, a novel restriction site was introduced with each

Table 1. Sequence comparison (in %) of putative lumazine synthases from 30 bacterial, three fungal and three plant species

Position in <i>B. subtilis</i>	hydrophobic						polar						acidic		basic				
	Gly	Val	Ala	Leu	Ile	Phe	Trp	Tyr	Ser	Thr	Cys	Met	Asn	Gln	Asp	Glu	Lys	Arg	His
<i>Phe22</i>						78	22												
<i>Ala56</i>		6	58		25				8		3								
<i>Phe57</i>					5	56	11	25			3		3						
<i>Phe61</i>		17		36	14	14	3	5	3		5			3					
<i>Val81</i>		75		19	6														
<i>Ile82</i>		8			92														
<i>Val92</i>		81			19														
<i>Phe113</i>					19		67		6				8						
<i>Asn23</i>										3			86						11
<i>Thr80</i>		28	33	3		3	11		3	19									
<i>Ser142</i>	5	8	28						17	28		3	3					8	
<i>Glu58</i>														11	89				
<i>Glu126</i>			5		3		3		3	3		3	8	5	5	56	3		3
<i>Asp138</i>	3	3							5					3	19	67			
<i>His88</i>																		6	94
<i>Arg127</i>																		94	6
<i>Lys131</i>	6								12					9		70			
<i>Lys135</i>					6											72	11	11	

Italic, amino acids which interact with their side chains; regular type, amino acids which interact with their main chain atoms.

mismatch primer used for mutagenesis (Table 6, Figure 7). Thus, the resulting plasmids could be checked by restriction analysis, which confirmed the presence of the respective novel restriction site. All mutations were also confirmed by DNA sequencing.

Preliminary enzyme assays in crude cell extracts showed that the various amino acid replacements

had resulted in proteins with relative specific activities ranging from about 100 to less than 1% (Table 2). Since we were predominantly interested in the specific catalytic role, if any, of individual polar amino acid side-chains in proton transfer reactions, the mutant protein with the largest relative activity was selected for further study for each polar amino acid position. Thus, 19 mutant

Table 2. Approximate reaction rates (% of wild-type enzyme activity) of mutant lumazine synthases

	Gly	Val	Ala	Leu	Phe	Trp	Tyr	Ser	Thr	Cys	Asn	Gln	Asp	Glu	Lys	Arg	His
<i>Phe22</i>						39	91	40					12		6	12	
<i>Ala56</i>								69									
<i>Phe57</i>								36									
<i>Phe61</i>								8									
<i>Val81</i>					3												
<i>Ile82</i>								8									
<i>Val92</i>				23													
<i>Phe113</i>				3		25		5							2	3	
<i>Asn23</i>		<1						20				10					
<i>Thr80</i>		47						69			54		3				
<i>Ser142</i>	17		92	53						57			55				
<i>Glu58</i>								3				62	100				
<i>Glu126</i>			49														
<i>Asp138</i>			78														
<i>His88</i>			10		6			12						7	3	12	
<i>Arg127</i>			2	2				<1	<1		2		5	2	9		62
<i>Lys131</i>			<1								8			3		25	
<i>Lys135</i>			14								18			5			27

Catalytic activities were measured in crude cell extract of recombinant *E. coli* strains. Mutants that were selected for detailed kinetic measurements are deposited in bold.

Table 3. Steady state kinetic parameters of lumazine synthase mutants

Mutant	K_M 1 ^a (μM)	K_M 2 ^b (μM)	k_{cat} (s^{-1})
Wild type	54.66 \pm 5.65	8.57 \pm 1.44	0.0557 \pm 0.0014
Phe22Val	124.39 \pm 15.48	10.72 \pm 1.26	0.0147 \pm 0.0014
Phe22Ser	137.34 \pm 14.44	140.46 \pm 46.48	0.0263 \pm 0.0011
Phe22Asp	674.82 \pm 121.32	720.54 \pm 49.51 ^c	0.0081 \pm 0.0003
Phe22Trp	59.83 \pm 9.84	6.12 \pm 1.33	0.0244 \pm 0.0048
Asn23Ser	58.08 \pm 7.06	11.91 \pm 3.55	0.0122 \pm 0.0022
Ala56Ser	70.15 \pm 6.09	4.20 \pm 0.20	0.0453 \pm 0.0029
Phe57Ser	80.07 \pm 19.59	34.49 \pm 6.88	0.0244 \pm 0.0035
Glu58Gln	146.03 \pm 11.97	173.24 \pm 40.09	0.0391 \pm 0.0029
Thr80Val	41.96 \pm 6.02	4.06 \pm 0.67	0.0307 \pm 0.0054
His88Ala	60.12 \pm 15.88	146.53 \pm 40.20	0.0067 \pm 0.0003
His88Lys	42.19 \pm 12.13	55.57 \pm 10.65	0.0022 \pm 0.0003
Phe113Ser	66.45 \pm 12.13	278.48 \pm 98.15	0.0038 \pm 0.0008
Arg127Thr	ND	ND	<0.0008
Arg127His	3137.53 \pm 678.29	84.92 \pm 12.20	0.0388 \pm 0.0035
Lys131Asn	282.52 \pm 46.95	35.52 \pm 10.61	0.0054 \pm 0.0011
Lys131Arg	49.98 \pm 3.08	13.79 \pm 4.49	0.0166 \pm 0.0003
Lys135Ala	166.63 \pm 14.45	11.48 \pm 1.13	0.0122 \pm 0.0005
Asp138Ala	63.64 \pm 6.49	9.96 \pm 2.46	0.0510 \pm 0.0067
Ser142Leu	90.52 \pm 13.47	11.48 \pm 1.50	0.0347 \pm 0.0011

^a K_M 1: K_M for 3,4-dihydroxy-2-butanone 4-phosphate.

^b K_M 2: K_M for 5-amino-6-ribitylamino-2,4 (1*H*,3*H*)-pyrimidinedione.

^c Hill-coefficient, $n = 3.6$.

proteins (Table 3) were purified to apparent homogeneity.

The k_{cat} values of the selected mutants were in the range of 3.4–78% by comparison with the wild-type enzyme (Table 3). The K_M value for 3,4-dihydroxy-2-butanone 4-phosphate (**1**) varied between 42 μM and 3140 μM as compared to a value of 55 μM for the wild-type enzyme. The K_M value for 5-amino-6-ribitylamino-2,4(1*H*,3*H*)-pyrimidinedione (**2**) varied between 4 μM and 720 μM as compared to a value of 9 μM for the wild-type protein.

Replacement of polar amino acid residues interacting with the ribityl side-chain (Glu58, Ser142) had little influence on the kinetic rate, and even the K_M value for the ribitylamino-pyrimidine type substrate changed only by a factor of 3 or less. Apparently, the binding of the substrate results from the sum of individually small contributions by various structural motifs (amino acid side-chain and peptide backbone) of the protein, where the modification of an individual amino acid has only a minor impact. Moreover, the hydrophilic and hydrophobic interactions with the backbone may be more important than the interactions of the ribityl side-chain with amino acid side-chains.

The replacement of Phe22, whose phenyl ring forms a coplanar complex with the pyrimidine substrate **2**, has little impact on the maximum reaction velocity. Whereas that is not surprising in case of the Phe22Trp substitution because tryptophan is found in that position in the lumazine synthases of many organisms and is known to form a coplanar complex with the heterocyclic substrate, even the replacement of Phe22 by aliphatic (Phe22Val mutant) or polar side-chains (Phe22Asp, Phe22Ser mutants) reduces k_{cat} by less than a factor of 10.

The polar replacements increase the K_M for the pyrimidine substrate by factors of 18 (Phe22Ser mutant) and 80 (Phe22Asp mutant), respectively; obviously, the π complex involving the phenylalanine side-chain and the pyrimidine ring contribute to some extent to the binding affinity.

The replacement of Phe22 by either an aliphatic residue (valine) or by polar/charged residues (serine, aspartate) can also increase the K_M for the second substrate, 3,4-dihydroxy-2-butanone 4-phosphate (**1**), by more than an order of magnitude. The influence of the phenylalanine side-chain on the affinity to the carbohydrate phosphate is not easily explained by the three-dimensional structures of the enzyme. Interestingly, the Phe22Asp mutant shows positive cooperativity (Hill coefficient, 3.6) for the pyrimidine substrate, which was not observed with the wild-type and the other mutants studied. It should be mentioned that this mutant was not able to bind 6,7-bis(trifluoromethyl)-8-ribityllumazine hydrate as shown by ¹⁹F NMR ligand perturbation studies.²⁶

Replacement of Lys131, which forms an ion pair network including Glu126 and Arg127, by the neutral asparagine, reduces k_{cat} by a factor of 13; the more conservative Lys131Arg mutant retains one fourth of the wild-type catalytic activity. The K_M for **1** is increased about sixfold in the Lys131Asn mutant and about 57-fold in the Arg127His mutant, in line with the proposed role of Lys131 in substrate binding. Interestingly, however, K_M for the pyrimidine substrate **2** is also increased by replacement of the positively charged side-chains, although that would not have been obvious from the three-dimensional structure.

His88 is probably the most interesting case in terms of the hypothetical mechanism in Figure 3.

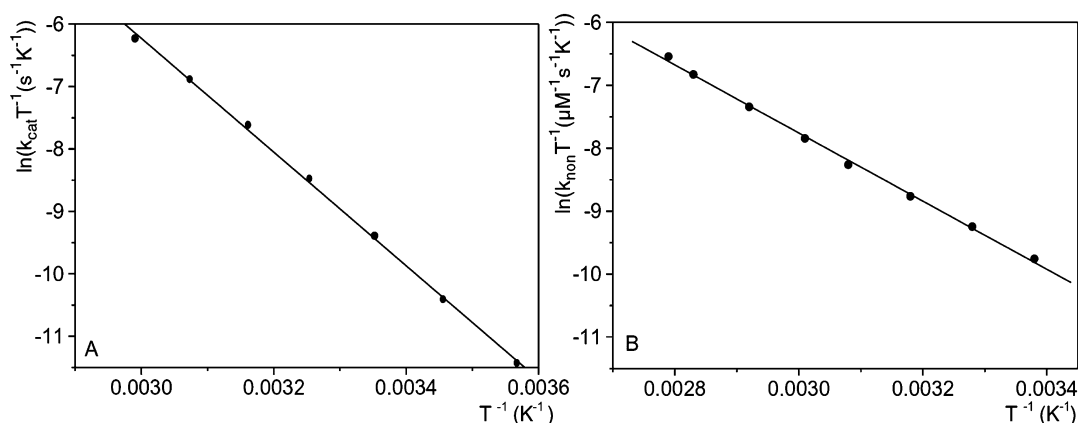


Figure 6. Eyring plots based on steady-state kinetic analysis. (a) Reaction catalysed by lumazine synthase of *B. subtilis*; (b) uncatalysed reaction.

Based on its proximity to the phosphoester side-chain of the Schiff base 5, the amino acid appeared ideally suited to abstract a proton from that side-chain as a prelude to the elimination of the phosphate residue.²³ Moreover, the histidine residue could assist in the subsequent enolisation of 6 by protonation of the methylene group and/or deprotonation of the enolic hydroxy group in 6.

The replacement of His88 by various amino acids resulted in fivefold to 30-fold reduced k_{cat} values. Specifically, the His88Ala mutant had a k_{cat} of 10% as compared to wild-type activity. The K_{M} for the pyrimidine substrate 2 is increased sixfold and 15-fold upon replacement of His88 by lysine and alanine, respectively.

The impact of replacing Phe113 by the less bulky serine is similar in its impact on velocity, which is reduced about tenfold, although the side-chain of Phe113 is not in direct contact with either substrates. The reduced velocity is accompanied by a 30-fold decrease in affinity for the pyrimidine type substrate. Hence it appears likely that the phenyl-alanine residues 57 and 113 are both important for holding the pyrimidine ring in the most appropriate position for the nucleophilic attack on the carbonyl group of 1.

In summary, our data show that the penalty, in terms of k_{cat} and K_{M} values, for the replacement of any amino acid residue in direct contact with the substrates and/or intermediates of lumazine synthase is relatively mild. This raises the question for how the catalytic rate acceleration is achieved by the enzyme.

Recently, we could show that the formation of 6,7-dimethyl-8-ribityllumazine (3) from 5-amino-6-ribitylamino-2,4(1*H*,3*H*)-pyrimidinedione (2) and 3,4-dihydroxy-2-butanone 4-phosphate (1) can proceed in neutral, aqueous solution at room temperature with appreciable velocity.²⁷ Whereas the enzyme-catalysed condensation is strictly regio-specific, the regiospecificity of the uncatalysed reaction varies with temperature and pH. The analysis of that partial regiospecificity suggested that the uncatalysed reaction proceeds by partitioning *via* at least two pathways.²⁷

Thermodynamic measurements were performed in a temperature range of 10–90 °C. The interpretation of the data substantially benefits from the fact that the enzyme shows a high temperature stability. Using calorimetric melting curves Zhang *et al.* showed that the icosahedral assembly of the enzyme remains intact up to a temperature of 93.3 °C.²¹

Eyring plots of the enzyme-catalysed and the uncatalysed reactions are shown in Figure 6 and the corresponding thermodynamic parameters are summarised in Table 4. The activation enthalpy ΔH^{\ddagger} of the uncatalysed reaction is 45 kJ mol⁻¹ (Table 4, Figure 6). A significantly larger value of 76 kJ mol⁻¹ was found for the reaction catalysed by the *B. subtilis* enzyme. Similar values of 84 kJ mol⁻¹, 83 kJ mol⁻¹, respectively, 85 kJ mol⁻¹ have been reported for the reactions catalysed by the enzymes from spinach, *M. grisea* and *E. coli*, respectively.²⁸ On the other hand the entropic terms ($T\Delta S^{\ddagger}$) of the enzyme-catalysed reactions are characterised by values in the range of -7.0 kJ mol⁻¹ to +3.0 kJ mol⁻¹, while a value of -37.8 kJ mol⁻¹ is found for the uncatalysed reaction. Thus the catalytic efficacy of lumazine synthases may be predominantly caused by their influence on the entropic term $T\Delta S^{\ddagger}$ of ΔG^{\ddagger} of the reaction.

Discussion

In many cases, the replacement of certain active site amino acid residues reduces the velocity of enzyme-catalysed reactions by many orders of magnitude. By comparison, the catalytic activity of lumazine synthase has now been shown to be surprisingly resilient to exchange of active site residues in this comprehensive study, which was aimed at saturating the active site of the enzyme with mutations.

The activation parameters summarised in Table 4 suggest that catalysis by lumazine synthase is predominantly due to an increase in the entropic term ($T\Delta S^{\ddagger}$) of the free energy of activation (ΔG^{\ddagger})

Table 4. Activation parameters for the enzymatic and non-enzymatic formation of lumazine

Enzyme	ΔG^\ddagger (kJ mol ⁻¹)	ΔH^\ddagger (kJ mol ⁻¹)	$T\Delta S^\ddagger$ (kJ mol ⁻¹)	Source
<i>B. subtilis</i>	83 ± 1.0	76 ± 1.0	-6.7 ± 1.1	This study
<i>S. oleracea</i>	82 ± 0.4	84 ± 1.7	2.1 ± 1.7	28
<i>M. grisea</i>	80 ± 0.4	83 ± 2.9	2.9 ± 2.9	28
<i>E. coli</i>	82 ± 0.4	85 ± 4.2	2.9 ± 4.2	28
Non-catalysed	83 ± 0.5	45 ± 0.5	-37.8 ± 0.5	This study

as compared to the uncatalysed reaction. This may implicate that the enzyme acts mainly by controlling the topology of the reactants.

Recently, we showed by pre-steady-state kinetic analysis that phosphate elimination is not the rate-limiting step in the reaction catalysed by lumazine synthase.²⁹ Zheng *et al.*²⁸ have proposed that the rate-limiting reaction step could be the rotation of the position 5 side-chain of intermediate **6**, which must precede the ring closure. The energy barrier of that reaction should be similar to that for the rotation of a peptide bond, which can proceed spontaneously on the timescale of seconds at room temperature. Whereas the rotation of peptide bonds can be catalytically accelerated by peptide isomerases of the cyclophilin type, it is as yet unknown whether catalytic acceleration of the side-chain rotation occurs in the case of lumazine synthase.

Materials and Methods

Materials

6,7-Dimethyl-8-ribityllumazine (**3**) was synthesised by published procedures.¹⁶ 5-Amino-6-ribitylamino-2,4(1*H*,3*H*)-pyrimidinedione (**2**) was freshly prepared from 5-nitro-6-ribitylamino-2,4(1*H*,3*H*)-pyrimidinedione (**10a**)^{30,31} by catalytic hydrogenation.¹⁶ Recombinant 3,4-dihydroxy-2-butanone 4-phosphate synthase of *E. coli* was used for preparation of 3,4-dihydroxy-2-butanone 4-phosphate (**1**) as described.³² Restriction enzymes were from Pharmacia Biotech (Freiburg, Germany). T4

DNA ligase was from Gibco BRL (Eggenstein, Germany). Oligonucleotides were custom synthesised by MWG Biotech (Ebersberg, Germany). DNA fragments were purified with the GeneClean II Kit from Bio 101 (San Diego, CA). Nucleobond AX20 columns were from Macherey und Nagel (Düren, Germany), isopropyl β-D-thiogalactopyranoside was from Bissendorf Biochemicals (Hannover, Germany), Q-Sepharose was from Pharmacia Biotech (Freiburg, Germany), lysozyme was from Sigma (Munich, Germany), and bovine pancreas DNase I was from Boehringer (Mannheim, Germany).

Strains and plasmids

Bacterial strains and plasmids used here are summarised in Table 5.

DNA sequencing

Sequencing was performed by the Sanger dideoxy chain termination method³³ using a model 377A DNA sequencer from Applied Biosystems (Foster City, CA). Plasmid DNA was isolated from cultures (5 ml) of XL1 Blue strains grown overnight in LB medium containing ampicillin (150 mg l⁻¹) using Nucleobond AX20 columns from Macherey und Nagel (Düren, Germany).

Construction of a hyperexpression strain

The coding region of the *ribH* gene of *B. subtilis* was amplified by polymerase chain reaction (PCR) using the plasmid p602-BS-RibH³⁴ as template and the oligonucleotides ribH1 and ribH2 as primers (Table 6). The amplification product served as template in a second PCR

Table 5. Bacterial strains and plasmids used in this study

Strain or plasmid	Relevant characteristics	Source
<i>E. coli</i> strain XL-1-Blue	<i>recA1</i> , <i>endA1</i> , <i>gyrA96</i> , <i>thi-1</i> , <i>hsdR17</i> , <i>supE44</i> , <i>relA1</i> , <i>lac[F'</i> , <i>proAB</i> , <i>lacI</i> ^q <i>ZΔM15</i> , <i>Tn10(tet^r)</i>	35
<i>B. subtilis</i> strain BR151[pBL1]	Trp, Met, Lys	39
Plasmid pNCO113	Expression vector	40
Plasmid p602/22	Expression vector	41

Table 6. Oligonucleotides used for construction of expression plasmids

Designation	Endonuclease	Sequence
RibH-1		5' <u>GAGGAGAAATTAACCATGAATATCATACAAGGAAATTA</u> 3'
RibH-2	<i>Bam</i> HI	5' <u>TATTATGGATCCCCATGGTTATTTCGAAAGAACGGTTAAAGTTTG</u> 3'
P1	<i>Eco</i> RI	5' <u>CAATTTGAATTCATTAAGAGGAGAAATTAAC</u> TATG3'
M1(+E)	<i>Eco</i> RI	5' <u>GTGAGCGGATAACAATTTACACAG</u> 3'
M2 (ΔE)		5' <u>AGATATTTTCATTAAGAGGAGAA</u> 3'
M4(+B)	<i>Bam</i> HI	5' <u>CTGCAGGTCGACGGATCC</u> 3'

Recognition sites are underlined.

using the oligonucleotides P1 and ribH2 as primers. The amplicate was cleaved with the restriction enzymes *Bam*HI and *Eco*RI and ligated into the plasmid pNCO113 (Table 5), which had been treated with the same enzymes. The resulting plasmid pNCO-BS-RibH was transformed into *E. coli* XL1 Blue cells.³⁵ Transformants were selected on LB solid medium supplemented with ampicillin (150 mg l⁻¹). The plasmid construct was monitored by restriction analysis and by DNA sequencing.

Site-directed mutagenesis

The construction of each mutant gene required four PCR amplifications. The first PCR used the plasmid pNCO-BS-RibH as template and oligonucleotide-pairs M1(+E) and M3(+RS3) as primers (Table 6, Figure 7). The latter oligonucleotide contained a mismatch codon for the introduction of the respective mutation. The second PCR used plasmid pNCO-BS-RibH as template and the oligonucleotide pairs M2(Δ E) and M4(+B) as primers. The amplicates from the two PCR steps were mixed and subjected to PCR without additional primers. In the final step, the reaction mixture of step 3 was re-amplified using the oligonucleotides M1(+E) and M4(+B) as primers. The amplicates were purified, digested with *Eco*RI and *Bam*HI and ligated into plasmid pNCO113, which had been treated with the same restriction enzymes. The ligation mixture was transformed into *E. coli* XL1 Blue cells.

Protein purification

The recombinant *B. subtilis* strain BR151[pBL1]-p602-BS-ribH was grown aerobically as described.³⁴ Recombinant *E. coli* strains were grown in LB medium containing ampicillin (150 mg l⁻¹) at 37 °C. At an optical density (600 nm) of about 0.7, isopropylthiogalactoside was added to a final concentration of 2 mM, and the cells were incubated for five hours. Cells were harvested by centrifugation (Sorvall GS3 rotor, 4,200g, 15 minutes, 4 °C), and washed twice with 0.9% NaCl and stored at -20 °C.

Frozen cell mass was thawed in 50 mM potassium phosphate (pH 7.0), containing 0.5 mM EDTA, 0.5 mM sodium sulphite and 0.02 % sodium azide. The suspension was cooled on ice, ultrasonically treated and centrifuged (Sorvall SS34 rotor, 27,000g, 15 minutes, 4 °C). The supernatant was applied to a column of Q-Sepharose FF (3 cm \times 25 cm), which had been equilibrated with 20 mM potassium phosphate (pH 7.0). After washing with 100 ml of 20 mM potassium phosphate (pH 7.0), the protein was eluted with a linear gradient of 0.02–1.0 M potassium phosphate (pH 7.0) (total volume, 800 ml). Fractions were collected and concentrated by ultracentrifugation (Beckman 70 Ti rotor, 18 hours, 75,200g, 4 °C).

Estimation of protein concentration

Protein concentration was estimated by a modified Bradford procedure as reported.³⁶

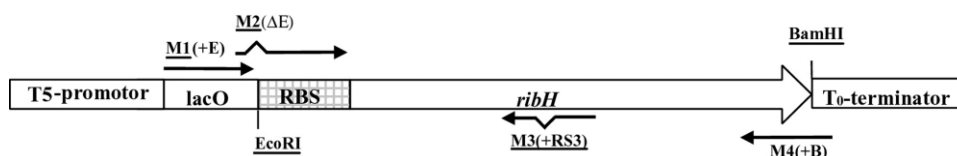


Figure 7. PCR-mediated site-directed mutagenesis. Primers are indicated by arrows.

SDS-polyacrylamide gel electrophoresis

Sodium dodecyl sulphate-polyacrylamide gel electrophoresis was performed as described.³⁷ Molecular mass standards were supplied by Sigma (Munich, Germany).

Steady-state kinetics

Assay mixtures contained 100 mM potassium phosphate (pH 7.0), 5 mM EDTA, 5-amino-6-ribitylamino-2,4-(1*H*,3*H*)-pyrimidinedione (2), 3,4-dihydroxy-2-butanone 4-phosphate (1) and protein in a total volume of 200 μ l.

In order to determine the K_M for amino-6-ribitylamino-2,4-(1*H*,3*H*)-pyrimidinedione (2) 1 μ M enzyme subunits were pre-incubated with various concentrations of 5-amino-6-ribitylamino-2,4-(1*H*,3*H*)-pyrimidinedione (2), starting with 5 μ M. The reaction was started by addition of 3,4-dihydroxy-2-butanone 4-phosphate (1) to a final concentration of 1 mM.

In order to estimate the K_M for 3,4-dihydroxy-2-butanone 4-phosphate (1) 5 μ M enzyme subunits were pre-incubated with increasing amounts of 3,4-dihydroxy-2-butanone 4-phosphate (1), starting with 10 μ M. The reaction was started by addition of 5-amino-6-ribitylamino-2,4-(1*H*,3*H*)-pyrimidinedione (2) to a final concentration of 1 mM.

Absorbance was monitored photometrically at 410 nm over 15 minutes at 37 °C. The concentration of the varying substrate was increased in the following assays until no change of reaction velocity (achievement of v_{max}) was observed. For each experiment a blank value without enzyme was determined under the same conditions. The initial rates of the blanks were subtracted from those of the corresponding enzymate experiments.

Corrected initial rates of the enzymatic measurements were fitted to the Michaelis Menten equation or the Hill equation using the program package Origin.

In the case of mutants with low activity the concentration of protein subunits was increased to 10–50 μ M.

Estimation of the thermodynamic parameters of the enzymatic and the non-enzymatic reaction

Reaction mixtures contained 5 μ M enzyme subunits, 1 mM of 5-amino-6-ribitylamino-2,4-(1*H*,3*H*)-pyrimidinedione (2) and 1.2 mM of 3,4-dihydroxy-2-butanone 4-phosphate (1) in 100 mM potassium phosphate (pH 7.0), 5 mM EDTA in a total volume of 200 μ l. The reaction was monitored at various temperatures (10–90 °C) as described above. The temperature inside the water-jacketed cuvettes was measured with a temperature sensor. Initial rates for the enzymatic reaction were corrected by a blank value measured under the same conditions without enzyme.

The rate constant for the non-enzymatic reaction (k_{non}) was determined from the initial rates of the blank values

Table 7. Accession numbers of mutant sequences submitted to GenBank

Mutant	Accession number	Mutant	Accession number	Mutant	Accession number	Mutant	Accession number
Phe22Val	AF516969	Phe61Ser	AF516973	Phe113Ser	AF516963	Lys131Glu	AF516983
Phe22Ser	AF516968	Thr80Val	AF517013	Phe113Lys	AF516961	Lys131Asn	AF516984
Phe22Asp	AF516965	Thr80Ser	AF517012	Phe113Arg	AF516962	Lys131Arg	AF516985
Phe22Lys	AF516966	Thr80Asp	AF517010	Phe113Trp	AF516964	Lys135Ala	AF516986
Phe22Arg	AF516967	Thr80Asn	AF517011	Glu126Ala	AF516954	Lys135Glu	AF516987
Phe22Tyr	AF516971	Val81Phe	AF517014	Arg127Ala	AF516996	Lys135Asn	AF516988
Phe22Trp	AF516970	Ile82Ser	AF516981	Arg127Leu	AF517001	Lys135Arg	AF516989
Asn23Val	AF516994	His88Ala	AF516975	Arg127Ser	AF517003	Asp138Ala	AF516952
Asn23Ser	AF516993	His88Ser	AF516980	Arg127Thr	AF517004	Ser142Gly	AF517009
Asn23Gln	AF516992	His88Glu	AF516976	Arg127Asp	AF516997	Ser142Ala	AF517006
Ala56Ser	AF516951	His88Lys	AF516978	Arg127Glu	AF516998	Ser142Leu	AF516950
Phe57Ser	AF516972	His88Arg	AF516979	Arg127Asn	AF517002	Ser142Asp	AF517008
Glu58Ser	AF516959	His88Phe	AF516977	Arg127Lys	AF517000	Ser142Cys	AF517007
Glu58Asp	AF516957	Val92Ala	AF517015	Arg127His	AF516999	wild type	AF516949
Glu58Gln	AF516958	Phe113Ala	AF516960	Lys131Ala	AF516982		

based on the kinetic equation for a second order reaction ($v = k_{\text{non}} \times c[\text{substrate1}] \times c[\text{substrate2}]$).

The thermodynamic parameters (ΔH^\ddagger , ΔS^\ddagger and ΔG^\ddagger) for the enzymatic and the non-enzymatic reaction were calculated from the corresponding Eyring plots using the relationships $\ln(kT^{-1}) = -\Delta H^\ddagger R^{-1} T^{-1} + \ln(k_b h^{-1}) + \Delta S^\ddagger R^{-1}$ and $\Delta G^\ddagger = \Delta H^\ddagger - T\Delta S^\ddagger$ with the program package Origin.

Analytical ultracentrifugation

Sedimentation equilibrium experiments were performed with an analytical ultracentrifuge Optima XL-A from Beckman Instruments (Palo Alto, CA) equipped with absorbance optics. Aluminium double-sector cells equipped with quartz windows were used throughout. Protein concentration was monitored photometrically at 280 nm. Protein samples were dialysed against 50 mM phosphate (pH 7.0). The partial specific volume was estimated from the amino acid composition, yielding a value of 0.742 ml g⁻¹.³⁸

Accession numbers

All sequences were deposited in GenBank (Table 7).

Acknowledgements

This work was supported by grants from the Deutsche Forschungsgemeinschaft, the Fonds der Chemischen Industrie and by NIH Grant GM51469. We thank A. Gießauf for help with some preliminary experiments. The expert help of A. Werner with the preparation of the manuscript is gratefully acknowledged.

References

- Oltmanns, O., Bacher, A., Lingens, F. & Zimmermann, F. K. (1969). Biochemical and genetic classification of riboflavin deficient mutants of *Saccharomyces cerevisiae*. *Mol. Gen. Genet.* **105**, 306–313.
- Shavlovsky, G. M., Teslyar, G. E. & Strugovshchikova, L. P. (1982). Regulation of flavogenesis in riboflavin-

dependent *Escherichia coli* mutants. *Mikrobiologiya*, **51**, 986–992.

- Shavlovskii, G. M., Ksheminskaia, G. P. & Strugovshchikova, L. P. (1968). Rate of flavinogenesis in *Candida guilliermondii* growing on media with a deficit of various nutrient substances. *Mikrobiologiya*, **37**, 591–599.
- Wang, A. (1992). Isolation of vitamin B2 auxotroph and preliminary genetic mapping in *Salmonella typhimurium*. *Yi Chuan Xue Bao*, **19**, 362–368.
- Gordon, S. V., Eiglmeier, K., Garnier, T., Brosch, R., Parkhill, J., Barrell, B. *et al.* (2001). Genomics of *Mycobacterium bovis*. *Tuberculosis*, **81**, 157–163.
- Young, D. W. (1986). The biosynthesis of the vitamins thiamin, riboflavin, and folic acid. *Nature Prod. Rep.* **3**, 395–419.
- Bacher, A., Eberhardt, S. & Richter, G. (1996). Biosynthesis of Riboflavin. In *Escherichia and Salmonella* (Neidhardt, F. C., Ingraham, J. L., Low, K. B., Magasanik, B., Schaechter, M. & Umberger, H. E., eds), vol. 1, pp. 657–664. 2 vols, American Society for Microbiology, Washington, DC.
- Bacher, A., Eberhardt, S., Eisenreich, W., Fischer, M., Herz, S., Illarionov, B. *et al.* (2001). Biosynthesis of riboflavin. *Vitam. Horm.* **61**, 1–49.
- Neuberger, G. & Bacher, A. (1986). Biosynthesis of riboflavin. Enzymatic formation of 6,7-dimethyl-8-ribityllumazine by heavy riboflavin synthase from *Bacillus subtilis*. *Biochem. Biophys. Res. Commun.* **139**, 1111–1116.
- Kis, K., Volk, R. & Bacher, A. (1995). Biosynthesis of riboflavin. Studies on the reaction mechanism of 6,7-dimethyl-8-ribityllumazine synthase. *Biochemistry*, **34**, 2883–2892.
- Maley, G. F. & Plaut, G. W. E. (1959). The isolation, synthesis and metabolic properties of 6,7-dimethyl-8-ribityllumazine. *J. Biol. Chem.* **234**, 641–647.
- Maley, G. F. & Plaut, G. W. E. (1959). The conversion of 6,7-dimethyl-8-ribityllumazine (6,7-dimethyl-8-ribityl-2,4(1H,3H)-pteridindione) to riboflavin by extracts of *Ashyba gossypii*. *J. Am. Chem. Soc.* **81**, 2025.
- Plaut, G. W. E. (1963). Studies on the nature of the enzymatic conversion of 6,7-dimethyl-8-ribityllumazine to riboflavin. *J. Biol. Chem.* **238**, 2225–2243.
- Wacker, H., Harvey, R. A., Winestock, C. H. & Plaut, G. W. E. (1964). 4-(1'-D-Ribitylamino)-5-amino-2,6-dihydroxypyrimidine, the second product of the riboflavin synthetase reaction. *J. Biol. Chem.* **239**, 3493–3497.
- Bacher, A., Baur, R., Eggers, U., Harders, H. D., Otto, M. K. & Schnepfle, H. (1980). Riboflavin synthases of

- Bacillus subtilis*. Purification and properties. *J. Biol. Chem.* **255**, 632–637.
16. Bacher, A. (1986). Heavy riboflavin synthase from *Bacillus subtilis*. *Methods Enzymol.* **122**, 192–199.
 17. Ladenstein, R., Schneider, M., Huber, R., Bartunik, H. D., Wilson, K., Schott, K. & Bacher, A. (1988). Heavy riboflavin synthase from *Bacillus subtilis*. Crystal structure analysis of the icosahedral beta 60 capsid at 3.3 Å resolution. *J. Mol. Biol.* **203**, 1045–1070.
 18. Kis, K. & Bacher, A. (1995). Substrate channeling in the lumazine synthase/riboflavin synthase complex of *Bacillus subtilis*. *J. Biol. Chem.* **270**, 16788–16795.
 19. Bacher, A., Ludwig, H. C., Schnepfle, H. & Ben Shaul, Y. (1986). Heavy riboflavin synthase from *Bacillus subtilis*. Quaternary structure and reaggregation. *J. Mol. Biol.* **187**, 75–86.
 20. Ritsert, K., Huber, R., Turk, D., Ladenstein, R., Schmidt Base, K. & Bacher, A. (1995). Studies on the lumazine synthase/riboflavin synthase complex of *Bacillus subtilis*: crystal structure analysis of reconstituted, icosahedral beta-subunit capsids with bound substrate analogue inhibitor at 2.4 Å resolution. *J. Mol. Biol.* **253**, 151–167.
 21. Zhang, X., Meining, W., Fischer, M., Bacher, A. & Ladenstein, R. (2001). X-ray structure analysis and crystallographic refinements of lumazine synthase from the hyperthermophile *Aquifex aeolicus* at 1.6 Å resolution: determinants of thermostability revealed from structural comparisons. *J. Mol. Biol.* **306**, 1099–1114.
 22. Persson, K., Schneider, G., Douglas, B. J., Viitanen, P. V. & Sandalova, T. (1999). Crystal structure analysis of a pentameric fungal and icosahedral plant lumazine synthase reveals the structural basis of differences in assembly. *Protein Sci.* **8**, 2355–2365.
 23. Meining, W., Mörtl, S., Fischer, M., Cushman, M., Bacher, A. & Ladenstein, R. (2000). The atomic structure of pentameric lumazine synthase from *Saccharomyces cerevisiae* at 1.85 Å resolution reveals the binding mode of a phosphonate intermediate analogue. *J. Mol. Biol.* **299**, 181–197.
 24. Gerhardt, S., Haase, I., Steinbacher, S., Kaiser, J. T., Cushman, M., Bacher, A. *et al.* (2002). The structural basis of Riboflavin binding to *Schizosaccharomyces pombe* 6,7-dimethyl-8-ribityllumazine synthase. *J. Mol. Biol.* **318**, 1317–1329.
 25. Braden, B. C., Vekilovsky, C. A., Cauerhff, A. A., Polikarpov, I. & Goldbaum, F. A. (2000). Divergence in macromolecular assembly: X-ray crystallographic structure analysis of lumazine synthase from *Brucella abortus*. *J. Mol. Biol.* **297**, 1031–1036.
 26. Scheuring, J., Kugelbrey, K., Weinkauff, S., Cushman, M., Bacher, A. & Fischer, M. (2001). 19F NMR ligand perturbation studies on 6,7-bis(trifluoromethyl)-8-ribityllumazine-7-hydrates and the lumazine synthase complex of *Bacillus subtilis*. Site-directed mutagenesis changes the mechanism and the stereoselectivity of the catalyzed haloform-type reaction. *J. Org. Chem.* **66**, 3811–3819.
 27. Kis, K., Kugelbrey, K. & Bacher, A. (2001). Biosynthesis of riboflavin. The reaction catalyzed by 6,7-dimethyl-8-ribityllumazine synthase can proceed without enzymatic catalysis under physiological conditions. *J. Org. Chem.* **66**, 2555–2559.
 28. Zheng, Y. J., Viitanen, P. V. & Jordan, D. B. (2000). Rate limitations in the lumazine synthase mechanism. *Bioorg. Chem.* **27**, 89–97.
 29. Schramek, N., Haase, I., Fischer, M., Bacher, A. (2002). Biosynthesis of riboflavin. Single turnover kinetic analysis of 6,7-dimethyl-8-ribityl-lumazine synthase. *J. Am. Chem. Soc.* In revision.
 30. Sedlmaier, H., Müller, F., Keller, P. J. & Bacher, A. (1987). Enzymatic synthesis of riboflavin and FMN specifically labeled with ¹³C in the xylene ring. *Z. Naturforsch. C*, **42**, 425–429.
 31. Cresswell, R. M. & Wood, H. C. S. (1960). The biosynthesis of pteridines. I. The synthesis of riboflavine. *J. Chem. Soc.*, 4768–4775.
 32. Richter, G., Krieger, C., Volk, R., Kis, K., Ritz, H., Gotze, E. & Bacher, A. (1997). Biosynthesis of riboflavin: 3,4-dihydroxy-2-butanone-4-phosphate synthase. *Methods Enzymol.* **280**, 374–382.
 33. Sanger, F., Niklen, S. & Coulson, A. R. (1977). DNA sequencing with chain-terminating inhibitors. *Proc. Natl Acad. Sci. USA*, **74**, 5463–5467.
 34. Braun, N., Tack, J., Fischer, M., Bacher, A., Bachmann, L. & Weinkauff, S. (2000). Electron microscopic observations on protein crystallization: adsorption layers, aggregates and crystal defects. *J. Cryst. Growth*, **212**, 270–282.
 35. Bullock, W. O., Fernandez, J. C. M. & Short, J. M. (1987). XL-blue: a high efficiency plasmid transforming recA *Escherichia coli* strain with β-galactosidase selection. *BioTechniques*, **5**, 376–379.
 36. Read, S. M. & Northcote, D. H. (1981). Minimization of variation in the response to different proteins of the Coomassie blue G dye-binding assay for protein. *Anal. Biochem.* **116**, 53–64.
 37. Laemmli, U. K. (1970). Cleavage of structural proteins during the assembly of the head of bacteriophage T4. *Nature*, **227**, 680–685.
 38. Laue, T. M., Shah, B. D., Ridgeway, T. M. & Pelletier, S. L. (1992). Computer-aided interpretation of analytical sedimentation data for proteins. In *Analytical Ultracentrifugation in Biochemistry and Polymer Science* (Harding, S. E., Rowe, A. J. & Horton, J. C., eds), pp. 90–125, Royal Society of Chemistry, Cambridge.
 39. Lovett, P. S. (1981). BR151ATCC 33677—*Bacillus subtilis* BR151. *J. Bacteriol.* **146**, 1162–1165.
 40. Stüber, D., Matile, H. & Garotta, G. (1990). System for high level production in *E. coli* and rapid purification of recombinant proteins: application to epitope mapping, preparation of antibodies and structure function analysis. In *Immunological Methods IV* (Lefkovits, I. & Pernis, P., eds), pp. 121–125.
 41. Henner, D. (1990). Expression of heterologous genes in *Bacillus subtilis*. Gene expression technology. *Methods Enzymol.* **185**, 199–228.

Edited by A. R. Fersht

(Received 14 August 2002; received in revised form 13 December 2002; accepted 13 December 2002)